First Multislit Collimator Prototype for SparseCT: Design, Manufacturing and Initial Validation

Baiyu Chen, Matthew J Muckley, Aaron Sodickson, Thomas O'Donnell, Matthias Berner, Thomas Allmendinger, Karl Stierstorfer, Thomas Flohr, Bernhard Schmidt, Daniel Sodickson, Ricardo Otazo[1]

***Abstract*— Compressed sensing represents a promising approach for CT dose reduction based on data undersampling. Alternative to reduced-view undersampling, which is difficult to implement, a within-view undersampling scheme named SparseCT has been proposed. SparseCT undersamples the beam within each view by interrupting the continuous beam with a multislit collimator (MSC). This work presents a SparseCT prototype, which to our knowledge is the first CS implementation on a clinical CT system. Details of the prototype design and manufacturing, data collection and processing steps, reconstruction steps unique to SparseCT, and initial phantom results are presented.**

***Index Terms*— CT, compressed sensing, SparseCT, prototype, undersampling, multi-slit collimator (MSC), penumbra**

I. Introduction

Compressed sensing (CS) is a promising technology for achieving order-of-magnitude CT dose reduction that uses undersampled projection data to reconstruct images [1]. The majority of CS studies have proposed a reduced-view undersampling scheme [1-3], which would require to pulse the x-ray tube to acquire reduced number of projections. However, this scheme is not feasible on a current clinical CT system, because the x-ray tube cannot be pulsed on the order of milliseconds due to the thermal inertia of the cathode.

We have developed an alternative to reduced-view undersampling, named SparseCT, which performs within-view undersampling [4, 5]. SparseCT does not pulse the x-ray beam, but instead interrupts the continuous beam with a multi-slit collimator (MSC). The MSC undersamples projection data within the view along the detector row direction (Figure 1). Furthermore, the MSC is jittered as the gantry rotates to change the undersampling pattern for each view to increase incoherence in the acquisition to improve the performance of compressed sensing.

Recently, we have built a SparseCT prototype, which to our knowledge is the first CS implementation on a clinical CT system. This work presents details of the prototype design and manufacturing, data collection and processing steps, a reconstruction algorithm tailored to SparseCT, and initial phantom results.

This work was supported by the National Institutes of Biomedical Imaging and Bioengineering under Grant U01 EB018760.

Baiyu Chen (e-mail: Baiyu.Chen@nyumc.org), Matthew J Muckley, Daniel Sodickson, and Ricardo Otazo (e-mail: Ricardo.Otazo @nyumc.org) are with the Department of Radiology, NYU Langone Health, New York, NY USA.

Thomas O'Donnell, Matthias Berner, Thomas Allmendinger, Karl Stierstorfer, Thomas Flohr, and Bernhard Schmidt are with Siemens Healthineers.

Aaron Sodickson is with Brigham and Women's Hospital, Boston, MA USA.

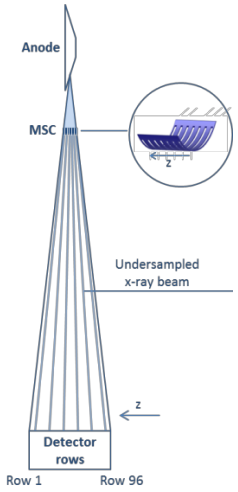

Figure 1: The multislit collimator (MSC) partially blocks the beam before it reaches the patient, such that undersampled projection data are acquired while reducing patient dose.

II. Methods

A. SparseCT prototype

The SparseCT prototype was designed and manufactured for the geometry of a Siemens SOMATOM Force scanner. The MSC was mounted onto the tube side of the scanner, 190 mm from the focal spot (Figure 2). The MSC is a tungsten plate curved along the fan angle and has laser-cut slits perpendicular to the z direction (patient bed direction). The plate is thick enough to block the beam so that the beam can only penetrate through the slits. The MSC can be moved along the z-direction with micrometer precision to undersample different detector rows.

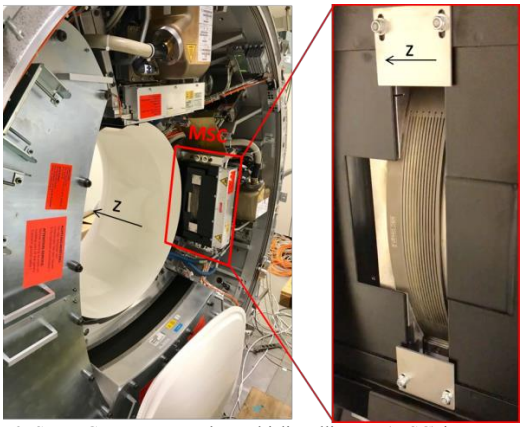

Figure 2: SparseCT prototype. The multislit collimator (MSC) is mounted to the tube side of the scanner and can be shifted along the z-direction.

Two MSC designs, named W4S12 and W4S16, were manufactured and tested on the prototype. "W" and "S" represent the slit width and the slit separation, respectively. For example, "W4S16" means that when projected to detector surface, each slit is 4-detector-row-wide and the separation between neighboring slits is 16-detector-row-wide. W4S12 and W4S16 have undersampling factors of 3 and 4, respectively.

The width of MSC slit was designed based on a previous study [5], which shows that the undersampled x-ray beam has penumbra regions on both sides of the beam, caused by the finite size of the focal spot (Figure **3**). The penumbra's width is independent of the slit width, about 3 rows on each side of the beam on detector surface. Consequently, as shown in Figure **4** (a simulation result from the previous study), the MSC slits need to be at least 3 to 4 rows wide (projected to detector surface) to ensure adequate separation between neighboring undersampled beam. Figure **4** also demonstrates that wider slits help reduce the amount of penumbra relative to umbra region, thus increasing dose efficiency. Based on aforementioned reasons, our prototype used a slit width of 4.

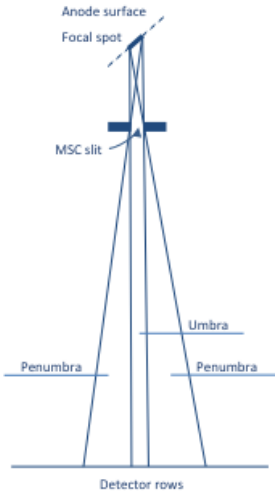

Figure 3: Due to the finite size of the focal spot, the beam through the MSC contains penumbra.

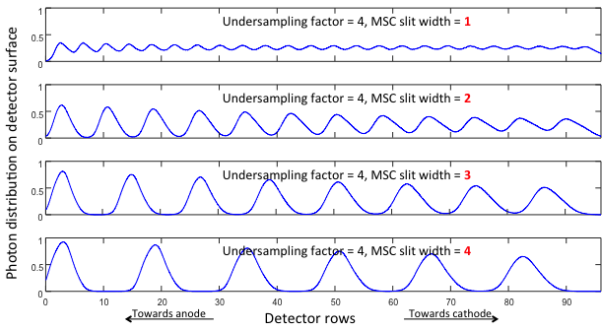

Figure 4: The photon distribution on the detector surface with different MSC designs, normalized by the photon distribution without MSC. All designs have the same undersampling factor of 4 but different slit width.

B. *Collection of Projection Data*

Both air scans and phantom scans were performed using the MSC prototype. For all scans, data were collected in a "step-and-shoot" fashion. The MSC was shifted along the z-direction to a prescribed location before an axial scan was taken. For W4S12 design, because the slit separation is 12 detector rows (projected to detector surface), we repeatedly scan at 12 different locations, each shifting the beam coverage by one row on the detector surface. For W4S16 design, scans were performed similarly at 16 different locations. All scans used a tube voltage of 120 kVp, a tube current of 800 mA, and a rotation time of 0.5 s.

C. *Processing of Projection Data*

In addition to the common preprocessing steps (e.g., air calibration and beam hardening correction), the projection data went through three steps unique to SparseCT.

First, a "MSC calibration" was performed to remove the attenuation of the MSC from the projection data of the phantom scans. This was done by subtracting the post-log projection data of the air scans from the post-log projection data of the phantom scans acquired at the same MSC locations.

Second, statistical weights were estimated based on the flux information (without MSC, provided by the vendor) and the phantom scans, which were inversely proportional to the variance of the post-log projection data and were used for reconstruction [6], as detailed in the next section.

Last, "dynamic MSC" scans were created by retrospectively drawing projections from scans of all MSC positions and stitching them together. The stitched scans simulate a linear MSC movement during the scan, shifting the beam by one row per projection.

D. *Reconstruction of Projection Data*

The processed projection data were reconstructed iteratively using a penalized weighted least squares cost function with OS-Momentum algorithm [7]. The reconstruction was tailored to SparseCT in two aspects.

First, to use the portion of projection data acquired in the penumbra region with reduced flux, we applied statistical weights to the reconstruction. The statistical weights accounted for the dramatic variation of exposure and quantum noise in the penumbra region by giving noisy data of less fidelity lower weights.

Second, to solve the "partial source obstruction" problem illustrated and explained in Figure 5, we analytically calculated the effective focal spot location corresponding to each detector row for each MSC design and MSC position, and passed on that information to the ray projector of the reconstruction algorithm.

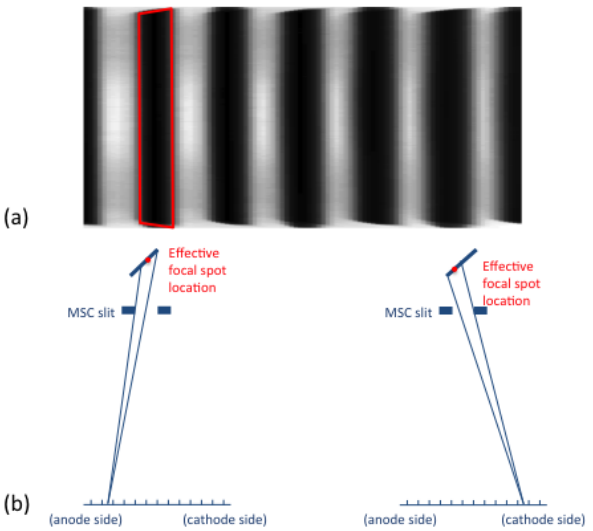

Figure 5: a) "Partial source obstruction" problem is when the projection of a SparseCT air scan captures each undersampled beam in trapezoidal shape instead of rectangular shape. b) This partial source obstruction is caused by the fact that the slit of the MSC is so narrow that part of the focal spot is obstructed by the slit. In other words, the detector rows in the beam can only "see" part of the focal spot. As a result, the effective locations of the focal spot (the centroid of the part of focal spot being seen) are different from row to row: The row on the anode side of the slit sees a focal spot further away from the MSC than the row on the cathode side of the slit, therefore having a smaller magnification ratio. Due to the difference in magnification ratio on the two sides of the beam, a rectangular beam was captured as a trapezoidal beam on the detector surface.

With these two aspects built into the reconstruction, the problem was formulated as the following optimization problem [8]:

$$\hat{\mathrm{x}} = \underset{\mathrm{x}}{\operatorname{argmin}} \frac{1}{2} \|\mathrm{y} - \mathbf{A}\mathrm{x}\|_{\mathrm{W}}^2 + \beta \sum_{m=1}^{M} \psi\left([\mathbf{C}\mathrm{x}]_m\right)$$

where x is the image to be reconstructed, y is the projection data, A is the data acquisition operator (gantry geometry and undersampling pattern), β is the regularization parameter that weights the sparsity term relative to data consistency, C is a finite difference operator, and ψ is a hyperbola function. The subscript "W" indicates the inclusion of statistical weights.

III. Results

A. Projection data

Figure 6 shows the projection data of a SparseCT phantom scan with W4S16 MSC, the projection data of a SparseCT air scan with W4S16 MSC at the same location, and the process of MSC calibration.

Note that the penumbra effect can be observed in Figure 6 (b), where the beam (the black strips) and the MSC (the white strips) do not have clear boundaries. Also note that although ¾ of the beam is interrupted by the W4S16 MSC, about ½ of the detector rows are irradiated due to the penumbra effect.

B. Reconstruction

Figure 7 shows the reconstructed images of a liver phantom with two low contrast lesions. All images were reconstructed with 350 mm FOV and 3 mm slice thickness. Figure 7(a) is the reference image acquired with full dose (no MSC) and reconstructed with Siemens WFBP algorithm. Figure 7(b) is the SparseCT image acquired with 1/3 dose (W4S12 MSC) and reconstructed with SparseCT algorithm. Figure 7(c) is SparseCT image acquired with ¼ dose (W4S16 MSC) and reconstructed with SparseCT algorithm.

Under reduced dose, SparseCT images still show the two low contrast lesions. However, ring artifacts are visible in the images, possibly because detector was calibrated for relatively uniform flux distribution, but the flux of the undersampled beam varies drastically across detector rows, even within a single row. In addition, the W4S16 result is noisy, which might be improved by changing the beta or the motion pattern of the MSC (currently a linear motion pattern was simulated).

IV. Conclusion

A prototype of SparseCT has been built, which to our knowledge is the first CS CT system based on a clinical system. Phantom data have been collected from the prototype. Special processing and reconstruction procedures have been developed and tested on the SparseCT data.

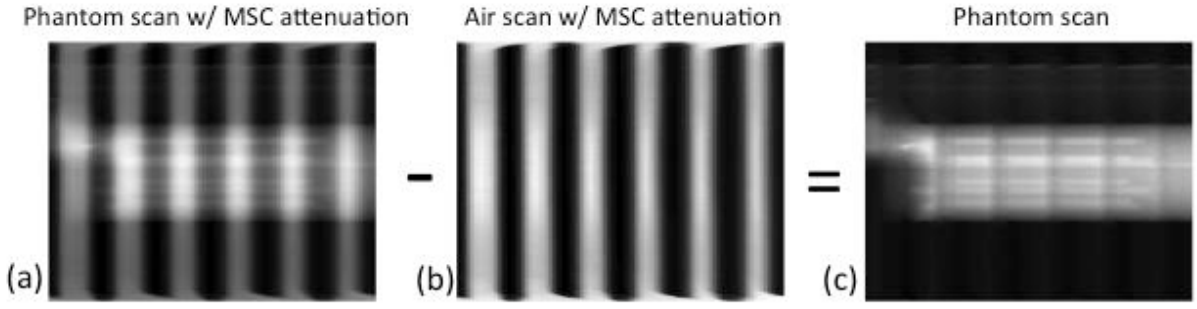

Figure 6: (a) A post-log projection of a SparseCT phantom scan with W4S16 MSC installed. The attenuation of the MSC is captured on top of the phantom attenuation in the projection. (b) A post-log projection of a SparseCT air scan with W4S16 MSC installed at the same location. (c) MSC calibration is performed by subtracting the aforementioned two, which removes the MSC attenuation from the projection.

ACKNOWLEDGMENT

This work was funded by National Institute of Biomedical Imaging and Bioengineering (U01 EB018760).

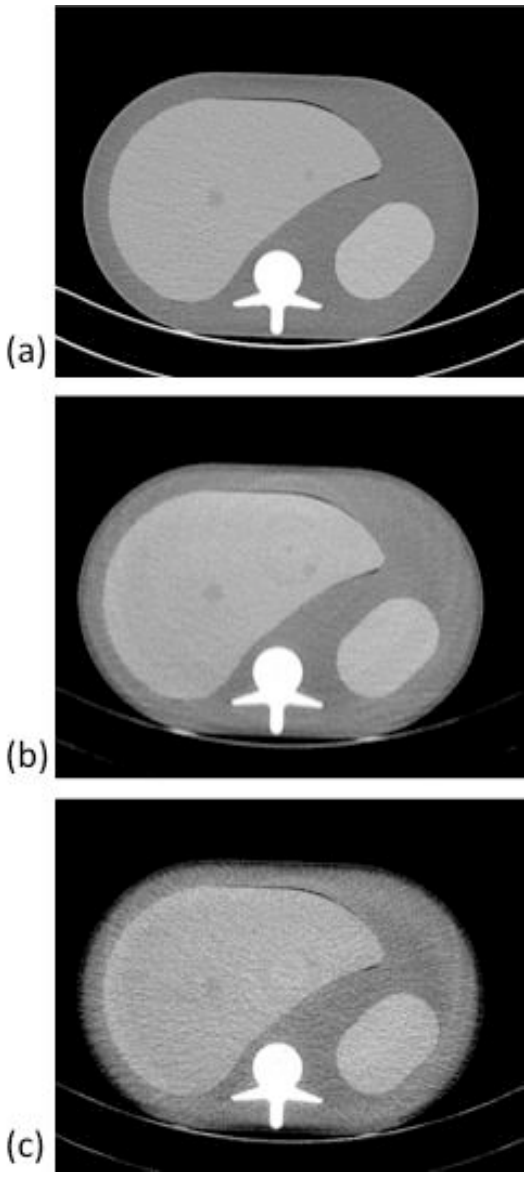

Figure 7: Reconstructed images of a liver phantom with two low contrast lesions: a) Full dose scan without MSC, WFBP reconstruction, b) 1/3 dose scan with W4S12 MSC, SparseCT reconstruction, and c) 1/4 dose scan with W4S16 MSC, SparseCT reconstruction.

REFERENCES

[1] G. H. Chen, J. Tang, and S. Leng, "Prior image constrained compressed sensing (PICCS): a method to accurately reconstruct dynamic CT images from highly undersampled projection data sets," *Med Phys,* vol. 35, pp. 660-3, Feb 2008.

[2] K. Choi, J. Wang, L. Zhu, T. S. Suh, S. Boyd, and L. Xing, "Compressed sensing based cone-beam computed tomography reconstruction with a first-order method," *Med Phys,* vol. 37, pp. 5113-25, Sep 2010.

[3] J. C. Ramirez-Giraldo, J. Trzasko, S. Leng, L. Yu, A. Manduca, and C. H. McCollough, "Nonconvex prior image constrained compressed sensing (NCPICCS): theory and simulations on perfusion CT," *Med Phys,* vol. 38, pp. 2157-67, Apr 2011.

[4] T. Koesters, F. Knoll, A. Sodickson, D. Sodickson, and R. Otazo, "SparseCT: Interrupted-beam acquisition and sparse reconstruction for radiation dose reduction," presented at the SPIE Medical Imaging, Orlando, FL, 2017.

[5] B. Chen, M. Muckley, T. O'Donnell, A. Sodickson, T. Flohr, K. Stierstorfer*, et al.*, "Realistic Undersampling Model for Compressed Sensing Using a Multi-Slit Collimator," presented at the The 14th International Meeting on Fully Three-Dimensional Image Reconstruction in Radiology and Nuclear Medicine, Xi'an, China, 2017.

[6] G. L. Zeng and W. Wang, "On Approximation of Compound Poisson by Poisson," presented at the The 4th International Conference on Image Formation in X-Ray Computed Tomography, 2016.

[7] D. Kim, S. Ramani, and J. A. Fessler, "Combining ordered subsets and momentum for accelerated X-ray CT image reconstruction," *IEEE Trans Med Imaging,* vol. 34, pp. 167-78, Jan 2015.

[8] M. Muckley, B. Chen, T. Vahle, A. Sodickson, F. Knoll, D. K. Sodickson*, et al.*, "Regularizer Performance for SparseCT Image Reconstruction With Practical Subsampling," presented at the The 14th International Meeting on Fully Three-Dimensional Image Reconstruction in Radiology and Nuclear Medicine, Xi'an, China, 2017.